Check for updates

ADVANCED ENGINEERING MATERIALS
www.aem-journal.com

Resistive Switching of Perovskite-Type Oxides Using the Hebb–Wagner Polarization Method

Nadja Ahr and Manfred Martin**

Resistive switching, the change between a high-resistive OFF state and a low-resistive ON state, is well known for thin film oxides sandwiched between two ion-blocking electrodes. Herein, the possibility for resistive switching in perovskite-type oxides using the Hebb–Wagner polarization setup that uses an ion-blocking and a reversible electrode is investigated. The resistive switching behavior is simulated numerically in terms of a defect chemical and transport model that describes the polarization of the model system $SrTiO_3$ between two different electrodes by applying an ac voltage. Corresponding experiments are also performed and the experimental results are compared with the simulation results. It is shown that the Hebb–Wagner setup allows the bulk resistive state to change not only for thin films but also for large sample thicknesses using low maximum voltage values, without the need for initially high voltages to form filaments. The effect of other parameters and phenomena on the switching behavior, like maximum voltage, surface exchange coefficient, sample thickness, and a Schottky contact between an electrode and the semiconducting oxide, is also determined. The experimental results show a high agreement with the numerical simulations, demonstrating that the Hebb–Wagner polarization setup enables bulk resistive switching of perovskite-type oxides.

1. Introduction

In the last 20 years, great progress in the development of electronic devices and nanotechnologies led to a high demand for nonvolatile data memories (NVM). As promising representatives of these NVMs, resistance random access memories (ReRAM) aroused a high interest in science and industry.[1–6] The memory function of the ReRAMs is based on electrically switchable resistance states that allow very fast switching times[7] and low write and read voltages.[2] The ReRAM cells consist typically of a resistive material that is attached to two electrodes. By applying an electroforming step, the material can be SET from a high-resistive OFF state to a low-resistive ON state. According to the current–voltage dependence, three different resistive switching modes are possible: 1) unipolar switching, which shows different required voltage and current values for the SET and RESET process; 2) bipolar switching, which needs different voltage polarities for either the SET or RESET process; and 3) abnormal bipolar switching, which shows the same behavior as the bipolar mode but is independent of the voltage polarity. There is a large number of effects which describe the change of the resistive state in different materials, for example, the electrochemical metallization effect, the molecular switching effect, and the valency change memory effect,[2] which will be discussed later. The research on the field of resistive switching materials started in the early 1960s with thin film oxide materials, that is, Al_2O_3, SiO_2, or TiO_2,[8–11] and today includes a variety of doped and undoped compounds, for example, perovskite-type oxides.[12,13] The transition metal oxide $SrTiO_3$ (STO) is a favored perovskite model system due to its well-known defect chemistry and high thermal and chemical stability.[14,15] Thus, it is hardly surprising that there are a lot of studies about the resistive switching behavior of unintentionally doped and doped $SrTiO_3$.[2,16–22] It is known that the resistance changes in STO are based on the migration of oxygen ions, which results in a change of the stoichiometry that causes a redox reaction affecting the electronic conductivity. This process is called the valency change memory effect and is typically connected to a bipolar switching behavior, where the polarity of the ac voltage defines the direction of the change, that is, the oxidation or reduction.[2]

STO is a so-called mixed ionic and electronic conductor (MIEC); this means that the partial conductivity depends on external parameters, such as temperature, oxygen partial pressure, and doping. The defect chemistry of STO is generally valid for many ABO_3 perovskites and in a temperature range between 773 and 1273 K it is defined by two reactions.[23] First, there is an oxygen exchange at the surface of the material, which is described by Equation (1), using Kröger–Vink notation.[24]

$$O_O^x \rightleftharpoons \frac{1}{2}O_2(g) + 2e' + V_O^{\cdot\cdot} \tag{1}$$

N. Ahr, M. Martin
Institute of Physical Chemistry
RWTH Aachen University
Landoltweg 2, 52074 Aachen, Germany
E-mail: nadja.ahr@rwth-aachen.de; martin@rwth-aachen.de

The ORCID identification number(s) for the author(s) of this article can be found under https://doi.org/10.1002/adem.202201741.

© 2023 The Authors. Advanced Engineering Materials published by Wiley-VCH GmbH. This is an open access article under the terms of the Creative Commons Attribution-NonCommercial-NoDerivs License, which permits use and distribution in any medium, provided the original work is properly cited, the use is non-commercial and no modifications or adaptations are made.

DOI: 10.1002/adem.202201741

The amount of oxygen in the material depends on the oxygen partial pressure (normalized to 1 bar) in the atmosphere. Assuming reductive conditions, the equilibrium shifts toward the product side and the amount of oxygen vacancies and the corresponding number of electrons in the material increases. Under oxidative conditions, electron holes become the dominant electronic species in the material. The relation between electrons and electron holes is defined by the band transfer equation (Equation (2)).

$$\text{nil} \rightleftharpoons e' + h^{\cdot} \tag{2}$$

The change of the dominant electronic species is denoted by a transition point (p–n transition) at a certain oxygen partial pressure that depends on the temperature T and the acceptor concentration $c_{Ac'}$. In addition to the upper two equilibrium reactions, the charge neutrality condition (Equation (3)) has to be considered. Here, n and p are the concentrations of electrons and electron holes, and $c_{V_O^{\cdot\cdot}}$ is the concentration of the oxygen vacancies.

$$n + c_{Ac'} = 2c_{V_O^{\cdot\cdot}} + p \tag{3}$$

As mentioned previously, the resistive switching behavior of $SrTiO_3$ is based on the motion of oxygen ions between the attached electrodes. This leads to a change of the oxygen concentration and thus to a change of the valence state of the transition metal cations, which affects the resistance of the material.[2] Thus, the change of the resistance requires the formation of a distinct gradient of the oxygen ions—neglecting the chemical constitution of the electrodes and space-charge regions at the material–electrode interface—which is typically realized by two ion-blocking electrodes (IBEs) preventing the oxygen exchange with the atmosphere. Another possibility to generate an oxygen ion gradient is the polarization of the material by using two different electrodes: 1) a reversible (RE), which allows the oxygen exchange; and 2) an IBE. For a dc voltage, this technique is called the Hebb–Wagner polarization method.[25,26] Usually, this method is used to measure the minority partial conductivity of a material, either electronic or ionic, by attaching a specific electrode that prevents the flux of the mobile ions or electronic defects, respectively. The application of an external voltage U_{appl} leads to a drift flux of the mobile species between the two electrodes and thus to a concentration gradient of the mobile species within the sample. Consequently, this gradient causes a diffusion flux in the opposite direction, which compensates the drift flux, and the total flux of the mobile species j_i converges toward a steady-state (index s) (Equation (4)).

$$(j_i)_s = 0 \tag{4}$$

Under this steady-state condition, the electrical current flowing through the sample is only carried by the species which are responsible for the minority partial conductivity. This condition enables the calculation of the partial conductivity of the unblocked mobile species from the steady-state $I-V$ curve.

The kinetics of the Hebb–Wagner polarization of perovskite-type oxides was described numerically in our previous publication and includes a comprehensive explanation of the defect chemistry of ABO_3 materials and the Hebb–Wagner polarization method.[27]

In this article, we now demonstrate the possibility to use the Hebb–Wagner polarization setup under the application of an ac voltage to generate a resistive switching behavior in perovskite-type oxides or $SrTiO_3$, respectively. The effect of various parameters on the resistive switching pattern, that is, surface exchange coefficient, maximum voltage, frequency, working temperature, sample thickness, acceptor concentration, and a Schottky barrier, is investigated using a numerical model and experimentally.

2. Transport Equations

The driving force for the flux of oxygen ions is the gradient of their electrochemical potential $\nabla\eta_{O^{2-}}$, which consists of the gradient of the electrochemical potential of the electrons $\nabla\eta_e$ and the gradient of the chemical potential of oxygen $\nabla\mu_O$ (Equation (5)). This leads to a drift flux of oxygen ions and a diffusion flux in the opposite direction. The total flux of the oxygen vacancies is described by Equation (6). The simulation was performed in terms of oxygen vacancies to use the p_{O_2}-independent diffusion coefficient of the oxygen vacancies $D_{V_O^{\cdot\cdot}}$.

$$\nabla\eta_{O^{2-}} \equiv (\nabla\mu_O + 2\nabla\eta_e) \tag{5}$$

$$j_{V_O^{\cdot\cdot}} = \frac{D_{V_O^{\cdot\cdot}} c_{V_O^{\cdot\cdot}}}{RT}(\nabla\mu_O + 2\nabla\eta_e) \tag{6}$$

Here, $c_{V_O^{\cdot\cdot}}$ is the concentration of the oxygen vacancies, R is the ideal gas constant, and T is the temperature. The temporal change of the oxygen vacancies is described in the first partial differential equation (PDE) (Equation (7)), which is based on Fick's second law.

$$\frac{\partial c_{V_O^{\cdot\cdot}}}{\partial t} + \nabla\left(\frac{D_{V_O^{\cdot\cdot}} c_{V_O^{\cdot\cdot}}}{RT}(\nabla\mu_O + 2\nabla\eta_e)\right) = 0 \tag{7}$$

To solve the PDE for $c_{V_O^{\cdot\cdot}}(x,t)$, one initial condition and two boundary conditions must be considered. Before the polarization starts ($t=0$), a homogenous distribution of the oxygen vacancies is assumed (Equation (8)). Here, $c^0_{V_O^{\cdot\cdot}}$ is the initial oxygen vacancy concentration.

$$c_{V_O^{\cdot\cdot}}(x, t=0) = c^0_{V_O^{\cdot\cdot}} \tag{8}$$

The IBE blocks the oxygen vacancy flux, which leads to a boundary condition at the cathode described by Equation (9).

$$j^{IBE}_{V_O^{\cdot\cdot}} = 0 \tag{9}$$

The oxygen exchange at the RE is limited by the surface exchange coefficient k_{chem}. The respective expression for the oxygen flux is given in Equation (10).

$$j^{RE}_{V_O^{\cdot\cdot}} = k_{chem} \cdot (c^0_{V_O^{\cdot\cdot}} - c^{RE}_{V_O^{\cdot\cdot}}) \tag{10}$$

The second PDE for the electrochemical potential is derived by assuming charge neutrality within the material, that is, the divergence of the total current density ∇i_{total} must be zero (Equation (11)).

© 2023 The Authors. Advanced Engineering Materials published by Wiley-VCH GmbH

15272648, 0, Downloaded from https://onlinelibrary.wiley.com/doi/10.1002/adem.202201741 by Rwth Aachen Hochschulbibliothe, Wiley Online Library on [06/06/2023]. See the Terms and Conditions (https://onlinelibrary.wiley.com/terms-and-conditions) on Wiley Online Library for rules of use; OA articles are governed by the applicable Creative Commons License

$$\nabla i_{\text{total}} = \nabla(i_{V_O^{\cdot\cdot}} + i_n + i_p) = 0 \tag{11}$$

In combination with the expression for the partial current density of the species i_i (Equation (12)), the second PDE (Equation (13)) follows from Equation (11).

$$i_i = -\frac{\sigma_i}{z_i F}\nabla\eta_i \tag{12}$$

$$0 = \nabla\left(\frac{\sigma_n + \sigma_p + \sigma_{V_O^{\cdot\cdot}}}{F}\nabla\eta_e + \frac{\sigma_{V_O^{\cdot\cdot}}}{2F}\nabla\mu_O\right) \tag{13}$$

Here, σ_i is the conductivity of the mobile species and F is the Faraday constant.

To generate the gradient of the electrochemical potential of electrons, the following boundary conditions at the IBE (Equation (14)) and RE (Equation (15)) have to be considered.

$$\eta_e^{\text{IBE}} = -F \cdot U_{\text{appl}} \tag{14}$$

$$\eta_e^{\text{RE}} = 0 \tag{15}$$

A comprehensive description of the numerical model and a summary of all required parameters corresponding to $SrTiO_3$ can be found in our previous article.[27]

A schematic setup of the Hebb–Wagner cell is shown in Equation (16).

$$\text{RE}, p_{O_2}^0 | SrTiO_3 | \text{IBE} \tag{16}$$

Here, $p_{O_2}^0$ is the oxygen partial pressure at the RE, fixed to the standard atmospheric pressure of 0.21 bar.

The unintentional acceptor dopant is assumed to be a triple positive charged cation. The time-dependent applied ac voltage was defined by a sinusoidal wave function (Equation (17)).

$$\Delta U_{\text{appl}} = U_{\max} \cdot \sin((2\pi f) \cdot t) \tag{17}$$

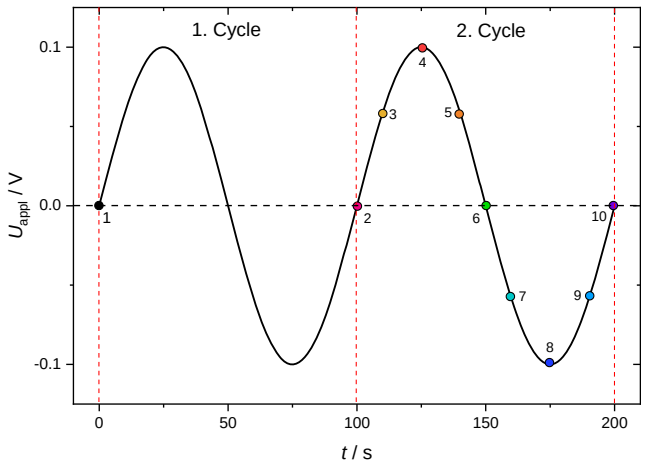


Figure 1. Applied voltage U_{appl} as a function of time t for two cycles at $U_{\max} = 0.1$ V and $f = 10^{-2}$ Hz. The numbered points on the voltage curve correspond to the examined times of the concentration profiles in this article.

The height of a cycle is set by the maximum voltage value $U_{\max}$ and the period of a cycle is defined by the required frequency f. The shape of the sinusoidal ac voltage is shown in **Figure 1**.

The voltage cycles are limited to two, with the second cycle to be studied in particular. For this purpose, different times, which correspond to the same voltage value, were selected within the second cycle to enable the comparison between the different resistive states (see numbered points in Figure 1). For the mesh of the finite element method, the cell was divided into 5000 elements with a maximal size of 6.7×10^{-5} m.

All required PDEs in this numerical simulation were solved using the finite element program COMSOL Multiphysics.[28]

3. Experimental Setup

A reasonable comparison between the numerical simulation and the experiments requires a simple setup of the Hebb–Wagner cell, which excludes the effect of grain boundaries. Thus, $SrTiO_3$ single crystals (Goodfellow, Hamburg, Germany) with a size of $1 \times 1 \times 0.05$ cm and a purity of 5 N (99.999%) were used. To realize the different electrodes, the RE and the IBE, a porous Au conducting paste and a Pt foil were used. The Pt foil was sintered to the single crystal by a conductive Au paste (Heraeus, Hanau, Germany) at 800 °C. The whole cell, except for the RE, was then covered with a high-temperature sealing glass (Schott AG, Landshut, Germany) to prevent the permeation of oxygen into the material. By connecting the prepared cells with the two probe Hebb–Wagner measuring station, a sinusoidal ac voltage could be applied to the $SrTiO_3$ single crystal using a waveform generator (Siglent SDG810, Shenzhen, CN). The measurement of the corresponding current density and the monitoring of the working temperature were performed with an oscilloscope (PicoScope 2204 A, St Neots, GB) and a multimeter (Keithley Series 2700, Cleveland, US).

4. Numerical Results

4.1. Hebb–Wagner Polarization Under Ideal Conditions

Assuming ideal conditions, classical Hebb–Wagner polarization implies a perfect oxygen exchange at the RE electrode and a complete blocking of ions at the IBE. Hence, the surface exchange coefficient at the RE is set to infinite in this section. The basis setup assumes a temperature of $T = 700$ °C, a sample thickness of $L = 1$ mm, and an acceptor concentration of $c_{Ac'} = 6 \times 10^{17}$ cm^{-3} (7 ppm). The maximum voltage $U_{\max}$ and the frequency f were changed until a distinct hysteresis in the $I - V$ curve could be observed (**Figure 2**). Starting at the origin of the $I - V$curve and applying a positive voltage at the IBE relative to the RE leads to a change of the material from the high-resistive OFF state (red curve) to the low-resistive ON state (black curve). This means that the corresponding current density i_{total} differs from a linear response and becomes significantly higher, which leads to a loop-like shape by lowering the voltage back to zero. This ON state is maintained also for negative voltages. Only when a certain negative voltage is applied, it switches back to the OFF state. This behavior is consistent with the bipolar switching mode and has already been observed by several research groups for the

© 2023 The Authors. Advanced Engineering Materials published by Wiley-VCH GmbH

15272648, 0, Downloaded from https://onlinelibrary.wiley.com/doi/10.1002/adem.202201741 by Rwth Aachen Hochschulbibliothe, Wiley Online Library on [06/06/2023]. See the Terms and Conditions (https://onlinelibrary.wiley.com/terms-and-conditions) on Wiley Online Library for rules of use; OA articles are governed by the applicable Creative Commons License

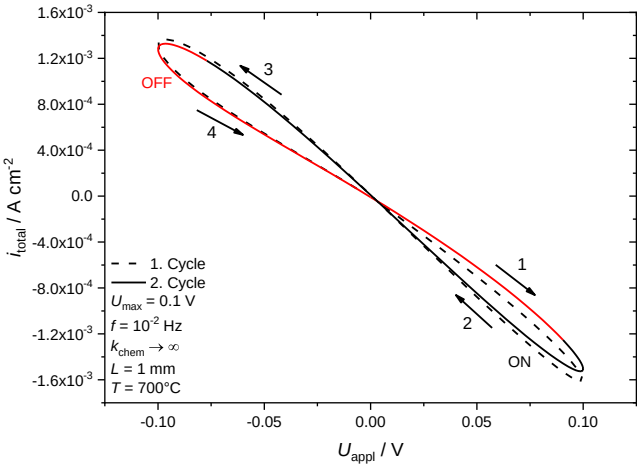


Figure 2. Simulated total current density i_{total} as a function of the applied voltage U_{appl} for two cycles at $U_{max} = 0.1$ V, $f = 10^{-2}$ Hz, $T = 700$ °C, $L = 1$ mm, $k_{chem} \rightarrow \infty$, and $c_{Ac'} = 6 \times 10^{17}$ cm^{-3}.

material $SrTiO_3$.[19,29–34] The direction of the hysteresis (the numbered arrows in Figure 2) corresponds to the Counter-Figure-8 polarity according to Waser et al.[35] Moreover, the hysteresis shows slightly different shapes for the first cycle (dashed line) in comparison to the second one (solid line). To find an explanation for the switching behavior, the species that contributes most to the total current density must be determined.

As we could show in our previous work,[27] the biggest contribution to the current density in this voltage range ($U_{max} = 0.1$ V) is due to the electronic defects (n + p). This assertion is verified in **Figure 3** that shows the different contributions to the total current density i_{total} by the electronic defects $i_{(n+p)}$ and the oxygen vacancies $i_{V\ddot{o}}$, averaged over the sample thickness. The amount carried by the oxygen vacancies is about two orders of magnitude lower compared to the amount of the electronic defects.

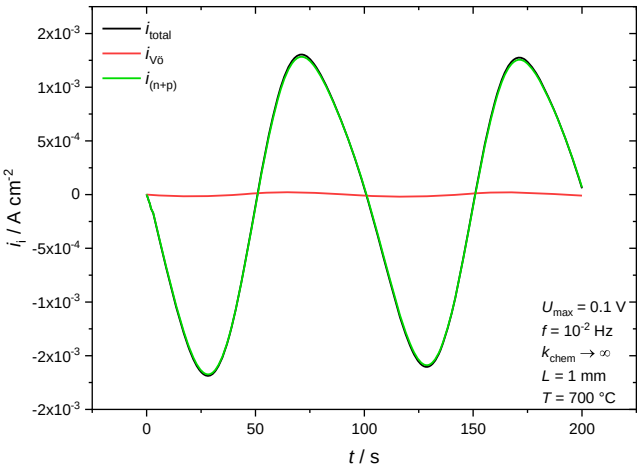


Figure 3. Simulated current densities i_i ($i = V_{\ddot{O}}$, $(n + p)$, and total) averaged over the sample thickness as a function of time t. The basic setup was used: $U_{max} = 0.1$ V, $f = 10^{-2}$ Hz, $T = 700$ °C, $L = 1$ mm, $k_{chem} \rightarrow \infty$, and $c_{Ac'} = 6 \times 10^{17}$ cm^{-3}.

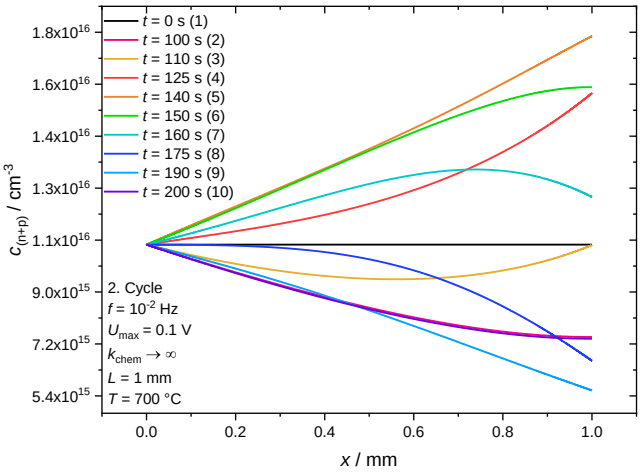


Figure 4. Simulated electronic concentration $c_{(n+p)}$ of the second voltage cycle as a function of position x within the sample at $U_{max} = 0.1$ V, $f = 10^{-2}$ Hz, $T = 700$ °C, $L = 1$ mm, $k_{chem} \rightarrow \infty$, and $c_{Ac'} = 6 \times 10^{17}$ cm^{-3}. The numbers correspond to the times marked in Figure 1.

Figure 4 shows the electronic concentration $c_{(n+p)}$ as a function of the position x within the sample for different times within the second voltage cycle, marked in Figure 1. Depending on the polarity on the IBE side of the sample ($x = 1$ mm), the applied voltage leads to a certain change of the electrochemical potential of the electrons η_e^{IBE} (see Equation (14) and Figure S1, Supporting Information) and thus to a change of the electronic concentration. At the RE ($x = 0$), the concentration of the electronic defects is fixed due to the perfect surface exchange. Consequently, a concentration gradient of the electronic defects within the sample is generated, which depends on the polarity of the applied voltage and the dominant electronic species. In the observed voltage range, the electron holes are the dominant species (p-type region).

The application of a positive voltage leads to an increase of the electron holes at the IBE and their flow toward the RE (see Equation (12)). A negative voltage results in the reverse behavior. The main reason for the switching behavior is the switching time, which is too short compared to the time required for the electron holes to fully relax.

As a result, the electronic concentration cannot relax fast enough after applying the first voltage half cycle (positive polarity) and does not reach the same constant initial value at $U_{appl} = 0$ V as at the beginning of the polarization. This leads to a gradient of the electronic concentration at a voltage of 0 V (noninitial zero-crossing), which is lower or higher as the initial value depending on the previous applied polarity (see $t = 100$ s, $t = 150$ s, and $t = 200$ s). This means that the positive voltage half cycle starts at a lower electronic concentration (cf., $t = 100$ s) and due to the high frequency, the concentrations before and after the maximum voltage differ from each other (cf., $t = 110$ s and $t = 140$ s). The concentration prior to the maximum is lower and thus leads to a lower current density or a high-resistive OFF state, while the concentration after the maximum is higher and leads to the low-resistive ON state. The opposite behavior can be observed for the voltage half cycle with the negative polarity. Moreover, the different noninitial zero-crossing concentrations explain the different shape of the $I - V$ curve of the first cycle.

© 2023 The Authors. Advanced Engineering Materials published by Wiley-VCH GmbH

15272648, 0, Downloaded from https://onlinelibrary.wiley.com/doi/10.1002/adem.202201741 by Rwth Aachen Hochschulbibliothe, Wiley Online Library on [06/06/2023]. See the Terms and Conditions (https://onlinelibrary.wiley.com/terms-and-conditions) on Wiley Online Library for rules of use; OA articles are governed by the applicable Creative Commons License

4.2. Effect of the Surface Exchange Coefficient and the Sample Thickness on the Resistive Switching Behavior

Under experimental conditions, it is not possible to achieve a perfect oxygen exchange at the RE electrode. It is thus necessary to include a surface exchange coefficient in the simulation model. For this purpose, an exchange coefficient of $k_{chem} = 7.2 \times 10^{-3}\,cm\,s^{-1}$, which corresponds to a Pt coated surface,[36] and a coefficient of $k_{chem} = 7.2 \times 10^{-5}\,cm\,s^{-1}$, which corresponds to the bare surface of $SrTiO_3$,[36] were assumed. The presence of a switching behavior strongly depends on the frequency and the sample thickness and varies for the different surface exchange coefficients. Thus, **Figure 5** illustrates the optimum frequency f_o to observe a switching behavior at a specific sample thickness.

Due to the different possible shapes of the hysteresis, a ratio between the ON and OFF state was defined to enable a clear comparison. The ratio of the states, that is, the amount of the current densities at the same voltage, must be around 1.3 (at $U_{max} = 0.08\,V$), which corresponds to the hysteresis shown in Figure 2. For small sample thicknesses ($L < 1\,mm$), the exchange coefficients lead to a significantly lower optimum frequency at the same sample thickness to generate a defined hysteresis. This means that the formation of a hysteresis at a sample thickness of $L = 10^{-2}\,mm$ and with a k_{chem} of about $10^{-5}\,cm\,s^{-1}$ takes about four orders of magnitude longer compared to the ideal exchange. This increase of the switching time fits well with the increase of the required relaxation time of the Hebb–Wagner polarization as discussed in our previous work.[27] Moreover, it can be observed that a very good surface exchange and a low sample thickness ($L = 10^{-4}\,mm$) leads to a very high optimum frequency ($f_o = 10^6\,Hz$). Furthermore, the surface exchange coefficient at low thicknesses leads to a weaker relation between sample thickness and frequency compared to the ideal exchange. This means that a limitation at the RE leads to a dependence that can be described by a proportionality of $\left(f \approx \frac{1}{L}\right)$, while an ideal exchange at the RE leads to a proportionality of $\left(f \approx \frac{1}{L^2}\right)$. These proportionalities are only observed at low thicknesses because the frequency–thickness relation of the surface-limited case changes to the relation of the ideal case at higher sample thicknesses. Here, the exact transition point depends on the surface exchange coefficient. For the higher coefficient ($k_{chem} = 7.2 \times 10^{-3}\,cm\,s^{-1}$), the transition occurs at $L = 1\,mm$ and for the lower coefficient ($k_{chem} = 7.2 \times 10^{-5}\,cm\,s^{-1}$) at $L = 100\,mm$. The proportionalities and the transitions indicate the change from surface control at low thicknesses to diffusion control at large thicknesses.

The lower optimum frequencies by including a surface exchange coefficient can again be explained by the concentration of the electronic defects. **Figure 6** shows the profiles of the electronic concentration considering the surface exchange coefficient of the bare $SrTiO_3$ surface at a frequency of $f = 10^{-2}\,Hz$ and a sample thickness of $L = 1\,mm$. This means that a distinct hysteresis cannot be observed under these conditions (cf., Figure 5). In comparison to the shape of the concentration curves under ideal conditions (see Figure 4), the initial value (black curve) cannot be reached at the RE. Moreover, the gradient of the transition points between the noninitial zero-crossings and the maximum voltage (cf., $t = 110\,s$ and $t = 140\,s$) is not as high as the gradient under ideal conditions. This is caused by an accumulation of the electronic species at the RE electrode due to the limited surface exchange. The accumulation leads to constant electronic concentrations when the voltage crosses the origin, which are also different from the initial value, but the distance at the IBE is smaller compared to the ideal conditions. As a result, the formation of the gradients in the ON and OFF state is weaker and switching behavior cannot be observed.

4.3. Effect of the Maximum Voltage and the Frequency on the Resistive Switching Behavior

A crucial parameter affecting the shape of the hysteresis significantly is the maximum applied voltage U_{max}. In **Figure 7**, the

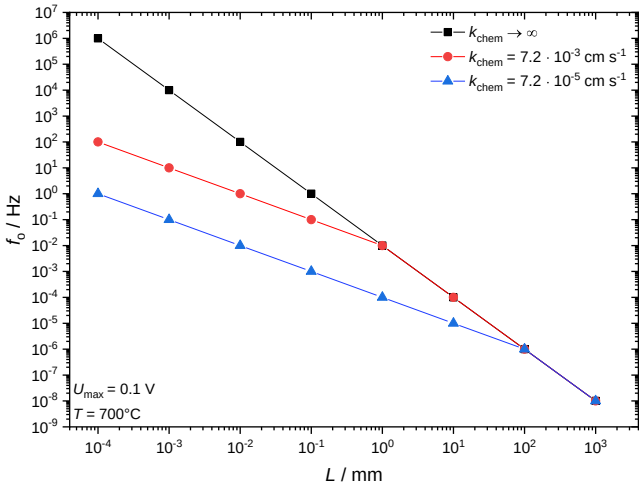


Figure 5. Optimum frequency f_o to generate a hysteresis during the second voltage cycle with an ON–OFF ratio of about 1.3 as a function of the sample thickness L for different surface exchange coefficients. The basic setup was used: $U_{max} = 0.1\,V$, $T = 700\,°C$, and $c_{Ac'} = 6 \times 10^{17}\,cm^{-3}$.

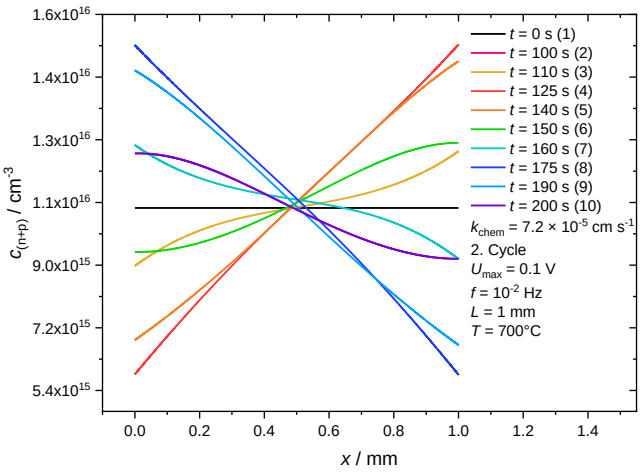


Figure 6. Simulated electronic concentration $c_{(n+p)}$ of the second voltage cycle as a function of position x within the sample at $U_{max} = 0.1\,V$, $f = 10^{-2}\,Hz$, $T = 700\,°C$, $L = 1\,mm$, $k_{chem} = 7.2 \times 10^{-5}\,cm\,s^{-1}$, and $c_{Ac'} = 6 \times 10^{17}\,cm^{-3}$.

© 2023 The Authors. Advanced Engineering Materials published by Wiley-VCH GmbH

15272648, 0, Downloaded from https://onlinelibrary.wiley.com/doi/10.1002/adem.202201741 by Rwth Aachen Hochschulbibliothe, Wiley Online Library on [06/06/2023]. See the Terms and Conditions (https://onlinelibrary.wiley.com/terms-and-conditions) on Wiley Online Library for rules of use; OA articles are governed by the applicable Creative Commons License

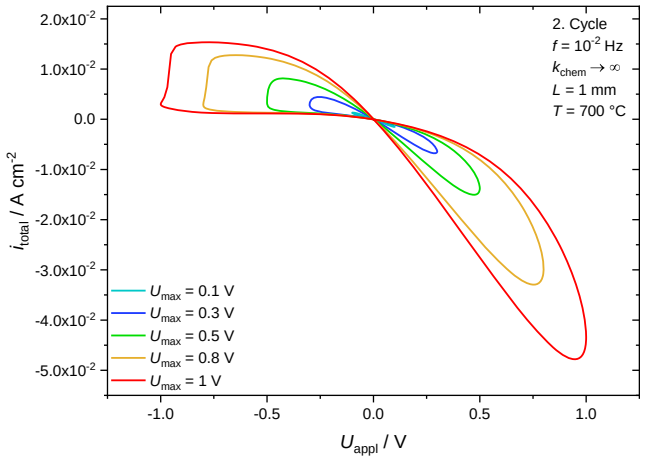


Figure 7. Simulated total current density i_{total} of the second cycle as a function of the applied voltage U_{appl} at different maximum voltages U_{max}. The basic setup was used: $f = 10^{-2}$ Hz, $T = 700$ °C, $L = 1$ mm, $k_{chem} \rightarrow \infty$, and $c_{Ac'} = 6 \times 10^{17}$ cm^{-3}.

total current density is plotted against the applied voltage for different maximum voltage values.

In the region of negative polarity, the ratio between the ON and OFF state becomes much higher and the required OFF voltage to switch to the high resistive state can be identified clearly by a distinct kink. In addition, from a maximum voltage of $U_{max} = 0.8$ V, there is a slight decrease in hysteresis around the maximum voltage value. The hysteresis with positive polarity also increases, but without showing a distinct kink as with negative voltages. The diagram also indicates that the maximum current density at positive voltages is about 3 times higher compared to the negative region.

A look on the electronic concentration at a maximum voltage of 1 V (**Figure 8**) explains the changed behavior for increasing voltages.

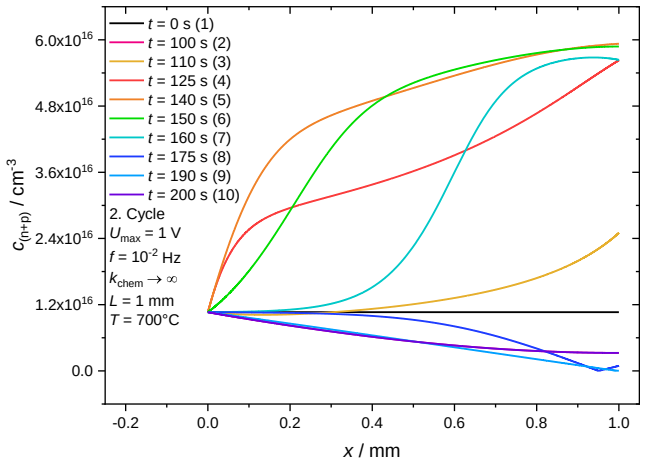


Figure 8. Simulated electronic concentration $c_{(n+p)}$ of the second voltage cycle as a function of position x within the sample at $U_{max} = 1$ V, $f = 10^{-2}$ Hz, $T = 700$ °C, $L = 1$ mm, $k_{chem} \rightarrow \infty$, and $c_{Ac'} = 6 \times 10^{17}$ cm^{-3}.

At positive voltages, the electronic concentration reaches a maximum value ($t = 140$ s), which depends on the amount of acceptor doping or the oxygen vacancy concentration. Due to the unhindered increase of the electronic concentration, the hysteresis grows without a significant change in the behavior. At negative voltages, the electronic concentration is limited by the p–n transition, which can be observed at the IBE for the maximum negative voltage value ($t = 175$ s). This means that the increase of the electronic defects is limited by the transition point and the current density is therefore smaller than in the positive voltage region. Moreover, the increase of the electronic defects beyond the p − n transition results in a smaller distance at the IBE between the initial value and the noninitial zero-crossing ($t = 0$ and $t = 200$ s), leading to a decrease of the hysteresis at the maximum voltage value.

The observation of a kink denoting the p − n transition agrees well with the results in our previous work,[27] where a dc voltage was applied to the Hebb–Wagner setup. This means that reducing the frequency gives the p − n transition more time to build up and thus shifts toward the RE (see **Figure 9**). This electrically induced p − n transition was first investigated by Weppner et al.[37] for a dc voltage. In addition, the continuous resistive switching behavior for different voltages without applying an initial high voltage shows that the Hebb–Wagner setup leads to a bulk switching mode instead of the filamentary switching often described in the literature.[18,38]

The effect of the frequency on the switching behavior at a maximum voltage of $U_{max} = 1$V is shown in **Figure 10**. The most pronounced hysteresis can be observed at a frequency of $f = 10^{-2}$Hz, while a change to higher or lower frequencies significantly reduces the hysteresis. This frequency value, which corresponds to a switching time of $t_{switch} = 100$ s, correlates with the relaxation time of the current density after an abrupt change of the dc voltage of around $t_{relax} = 40$ s that was determined for the same system in our previous work.[27] This means that the relaxation time of the Hebb–Wagner method and the switching time must be of the same order of magnitude to obtain a pronounced hysteresis. If the frequency is changed to higher values

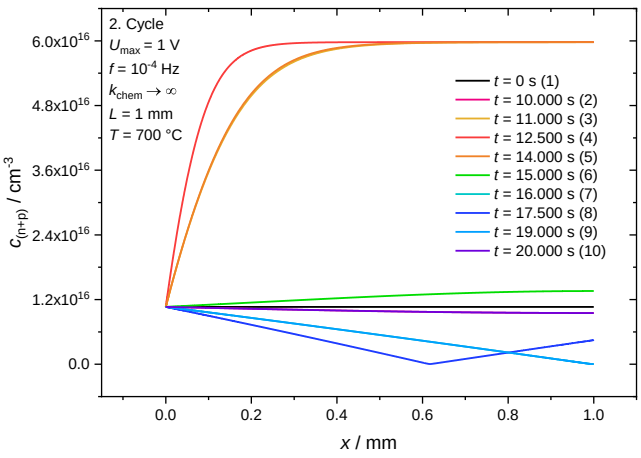


Figure 9. Simulated electronic concentration $c_{(n+p)}$ of the second voltage cycle as a function of position x within the sample at $U_{max} = 1$ V, $f = 10^{-4}$ Hz, $T = 700$ °C, $L = 1$ mm, $k_{chem} \rightarrow \infty$, and $c_{Ac'} = 6 \times 10^{17}$ cm^{-3}.

© 2023 The Authors. Advanced Engineering Materials published by Wiley-VCH GmbH

15272648, 0, Downloaded from https://onlinelibrary.wiley.com/doi/10.1002/adem.202201741 by Rwth Aachen Hochschulbibliothe, Wiley Online Library on [06/06/2023]. See the Terms and Conditions (https://onlinelibrary.wiley.com/terms-and-conditions) on Wiley Online Library for rules of use; OA articles are governed by the applicable Creative Commons License

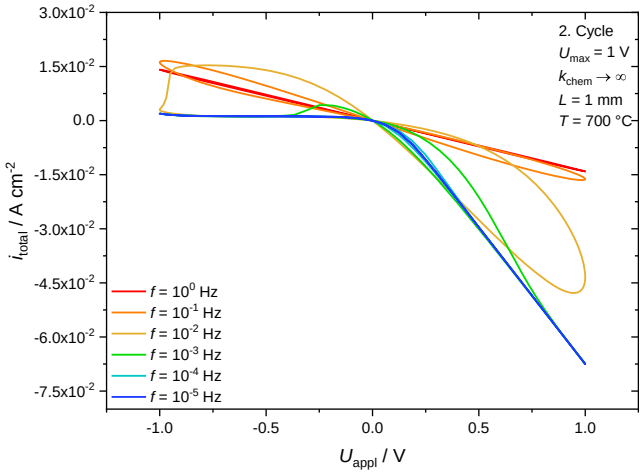


Figure 10. Simulated total current density i_{total} of the second cycle as a function of the applied voltage U_{appl} at different frequencies f. The basic setup was used: $U_{max} = 1$ V, $T = 700$ °C, $L = 1$ mm, $k_{chem} \rightarrow \infty$, and $c_{Ac'} = 6 \times 10^{17}$ cm^{-3}.

(lower switching times), the hysteresis becomes very small and turns into an Ohmic case, where the current density is independent of the polarity and the direction of the voltage (see red curve in Figure 10). This behavior is understandable because the switching time is not sufficient enough to generate a distinct gradient of the electronic defects within the sample.

By applying a lower frequency (higher switching time), the hysteresis becomes smaller in the positive region, while the hysteresis in the negative region shifts toward lower voltage values (green curve). Due to the lower frequency, the electron holes have more time to converge to the maximum possible concentration in the positive region, which leads to a reduction of the hysteresis. In the negative region, the lower frequency leads to a higher increase of the electronic concentration at the IBE and thus to a shift of the p − n transition point. This means that the difference at the IBE side becomes smaller and the hysteresis vanishes or shifts toward lower voltages. By applying a frequency of 10^{-5} Hz, the system has enough time to relax completely and the $I - V$ curve becomes equal to the typical Hebb–Wagner sinusoidal curve (blue curve) that would be observed for an applied dc voltage. Here, the plateau characterizing the p − n transition is found at negative voltages, while the increasing current density at positive voltages is due to the increase of the electron holes in this voltage range.[27]

In addition to the parameters already discussed, the effect of the working temperature and the acceptor concentration on the resistive switching behavior was also investigated. The corresponding results can be found in the supporting information.

4.4. Effect of a Schottky Barrier at the IBE on the Resistive Switching Behavior

A phenomenon that can have a big influence on the resistive switching behavior is a Schottky barrier at the electrode–semiconductor interface. Depending on the work function of the electrode and the semiconductor as well as on the polarity of the voltage and the dominant electronic species (n− type or p− type semiconductor), this Schottky barrier leads to an increase of the resistance at the interface and thus limits the current flow in a specific direction. This means that the effective voltage across the material is reduced as well as the resistive switching behavior. In our case, the work function of the electrodes (ϕ_{Pt}: 5.65 − 5.7 eV; ϕ_{Au}: 5.1 − 5.47eV)[39–41] is higher than the work function of the material (ϕ_{SrTiO_3}: 2.6 − 4.3 eV).[42–44] The dominant electronic species of $SrTiO_3$ depend on the oxygen partial pressure. For high partial pressures, the material can be described as a p− type semiconductor, while at low partial pressures, the material changes to a n− type semiconductor (see Figure S6, Supporting Information). This means that three different cases have to be considered: 1) the interface between the RE and a p− type semiconductor because the oxygen partial pressure at the RE is fixed to $p_{O_2} = 0.21$ bar; 2) the interface between the IBE and a p− type semiconductor at high partial pressures; and 3) the interface between the IBE and a n− type semiconductor at low partial pressures. In the first two cases, the p− type semiconductor results in an Ohmic contact that is independent of the polarity of the voltage. This means that a constant low resistance at the interface is possible, but it has no significant influence on the current. In the third case, a Schottky barrier must be taken into account, which increases the resistance of the electron transfer at the interface in dependence of the polarity of the voltage. Here, a positive voltage at the IBE relative to the RE defines the forward voltage, that is, the current is not hindered in this direction (except by a small resistance), while a negative voltage at the IBE defines the reverse voltage, so that the current flow is limited by a Schottky barrier. In the numerical model, a Schottky contact was implemented by using the following equation (Equation (18)).[45,46]

$$i = i_0 \cdot \left[\exp\left(\frac{eU_s}{k_b T} - 1\right)\right] \tag{18}$$

Here, i_0 is the saturation current, U_s is the voltage drop at the Schottky barrier, e is the elementary charge, and k_b is the Boltzmann constant.

The saturation current i_0 defines the magnitude of the resistance at the contact and thus affects the effective voltage or current within the sample. The distinct decrease of the effective voltage $U_{effective}$ in the negative polarity region at the IBE is shown in Figure S7, Supporting Information. To get an accurate impression of the effect of the Schottky barrier on the resistive switching behavior, **Figure 11** plots the total current density i_{total} as a function of the applied voltage U_{appl} at a maximum voltage of $U_{max} = 1$ V without and with a Schottky barrier. Furthermore, the dependence of the saturation current i_0 is also shown.

The limited current flow in the negative polarity region leads to a significant decrease of the hysteresis, which disappears completely as the saturation current decreases (see blue curve). The Schottky barrier also reduces the hysteresis in the positive polarity region, but the effect is much smaller. In summary, the presence of a Schottky barrier at the interface between the semiconductor and the electrode has a significant influence on the resistive switching behavior by reducing the effective voltage within the sample and thus the hysteresis. However, this effect

© 2023 The Authors. Advanced Engineering Materials published by Wiley-VCH GmbH

15272648, 0, Downloaded from https://onlinelibrary.wiley.com/doi/10.1002/adem.202201741 by Rwth Aachen Hochschulbibliothe, Wiley Online Library on [06/06/2023]. See the Terms and Conditions (https://onlinelibrary.wiley.com/terms-and-conditions) on Wiley Online Library for rules of use; OA articles are governed by the applicable Creative Commons License

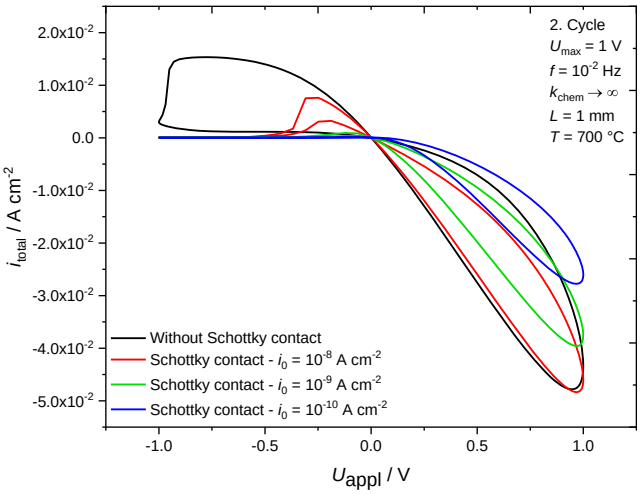


Figure 11. Simulated total current density i_{total} of the second cycle as a function of the applied voltage U_{appl} with different saturation currents i_0. The following setup was used: $U_{max} = 1$ V, $f = 10^{-2}$ Hz, $T = 700$ °C, $L = 1$ mm, $k_{chem} \rightarrow \infty$, and $c_{Ac'} = 6 \times 10^{17}$ cm^{-3}.

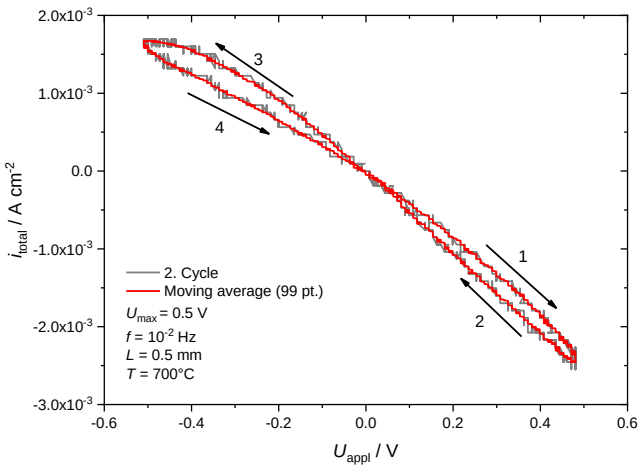


Figure 12. Experimental total current density i_{total} of the second cycle as a function of the applied voltage U_{appl}. The following experimental setup was used: $U_{max} = 0.5$ V, $f = 10^{-2}$ Hz, $T = 700$ °C, and $L = 0.5$ mm. The gray line represents the experimental measuring data, while the red line shows the smoothed data using a moving average fit with 99 points.

only needs to be considered at high voltages and, due to the p_{O_2} dependence, only at the IBE.

5. Experimental Results

To verify the results of the numerical simulation, a Hebb–Wagner measuring cell, including a $SrTiO_3$ single crystal, was connected to a waveform generator and polarized using an ac voltage. Various parameters, such as the maximum voltage U_{max} and the working temperature T, were changed to determine the dependencies between the resistive switching behavior and different experimental conditions. In **Figure 12**, the $I - V$ curve of the experiment at $U_{max} = 0.5$ V, $f = 10^{-2}$ Hz and $T = 700$ °C is shown. The red curve represents a moving average fit with 99 points to smooth the measuring data.

The data obtained from the resistive switching experiments show a distinct hysteresis, which depends on the polarity of the applied voltage. Moreover, the direction of the hysteresis follows the Counter-Figure-8 polarity. This means that the experimental switching curve corresponds to a bipolar Counter-Figure-8 behavior and thus fits well with the numerical simulations (see Figure 2).The shape of the hysteresis also shows a slightly higher ON–OFF (≈ 1.3 at $U_{appl} = -0.37$ V) and a lower maximum current density at negative voltages compared to the positive polarity region (ON–OFF ratio ≈ 1.2 at $U_{appl} = 0.34$ V). The main difference to the simulations is the maximum voltage, which must be higher in the experiment to observe a significant hysteresis. At a voltage of $U_{max} = 0.1$ V, for example, a hysteresis is shown as well, but the ratio is partly smaller than the resolution of the measuring devices. This becomes clear by looking at the $I - V$ curves at different U_{max} (**Figure 13**).

The current density rises with increasing voltages with the maximum current at positive voltages becoming higher as the current at negative voltages. Moreover, the ON–OFF ratio in the negative region increases with the voltage value and a sharper transition between the ON and OFF state at $U_{max} = 1$ V is indicated. In comparison to the simulations, this increase of the current density and the ratio is not high enough to see exactly the same switching behavior, especially at higher voltages above $U_{max} = 0.5$V.

Besides the influence of the maximum voltage U_{max}, the working temperature T was also investigated experimentally (**Figure 14**). The increase of the temperature leads to a small increase of the current density and a reduction of the ON–OFF ratio in both polarity regions. This corresponds to the results obtained from the numerical simulations (see Figure S4, Supporting Information) and is probably caused by the change of the mobilities of the involved species. However, the absolute values also deviate from those in the simulations.

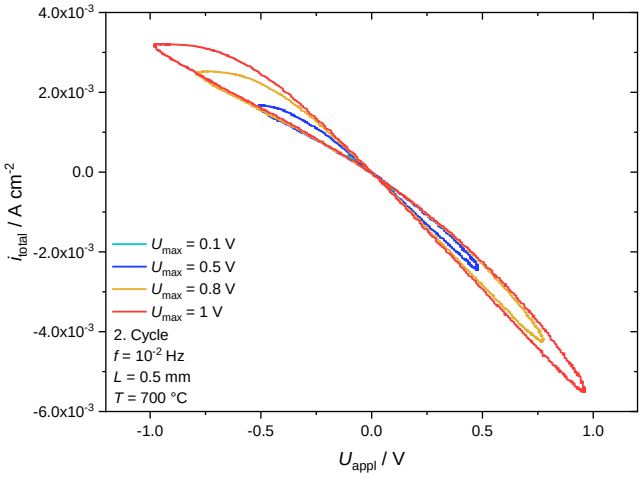


Figure 13. Experimental total current density i_{total} of the second cycle as a function of the applied voltage U_{appl} at different maximum voltages U_{max}. The following experimental setup was used: $f = 10^{-2}$ Hz, $T = 700$ °C, and $L = 0.5$ mm.

© 2023 The Authors. Advanced Engineering Materials published by Wiley-VCH GmbH

15272648, 0, Downloaded from https://onlinelibrary.wiley.com/doi/10.1002/adem.202201741 by Rwth Aachen Hochschulbibliothe, Wiley Online Library on [06/06/2023]. See the Terms and Conditions (https://onlinelibrary.wiley.com/terms-and-conditions) on Wiley Online Library for rules of use; OA articles are governed by the applicable Creative Commons License

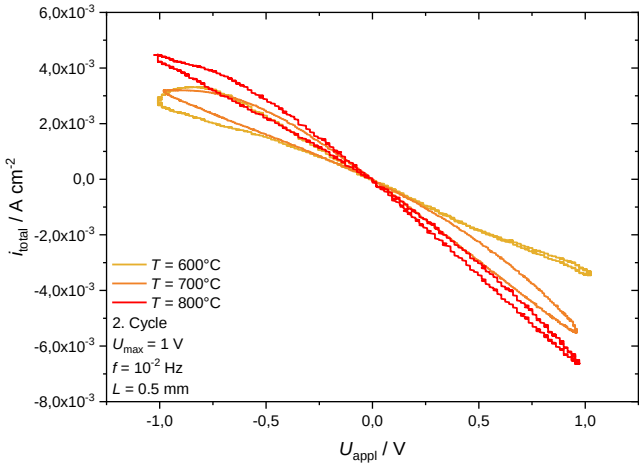


Figure 14. Experimental total current density i_{total} of the second cycle as a function of the applied voltage U_{appl} at different working temperatures T. The following experimental setup was used: $U_{max} = 1$ V, $f = 10^{-2}$ Hz, and $L = 0.5$ mm.

Nevertheless, it can be seen that the general behavior of the hysteresis and the effect of the varied parameters correspond well with the numerical simulations.

It is possible to approximately reproduce the experimental results by considering problems of the experimental realization, such as a limited oxygen exchange at the RE, a higher acceptor impurity of the single crystal, or an additional resistance within the measuring cell. Therefore, the numerical simulations were performed by introducing a surface exchange coefficient of $k_{chem} = 7.2 \times 10^{-3}$ cm s^{-1}, which corresponds to a Pt-coated surface at the RE,[36] an acceptor concentration of $c_{Ac'} = 1 \times 10^{18}$ cm^{-3}, a sample thickness of $L = 0.5$ mm, and a maximum voltage, which is one order of magnitude lower as in the experiment. The corresponding $I - V$ curves at different maximum voltages is shown in **Figure 15** (the reproduced $I - V$ curves at $U_{max} = 0.05$ V and at

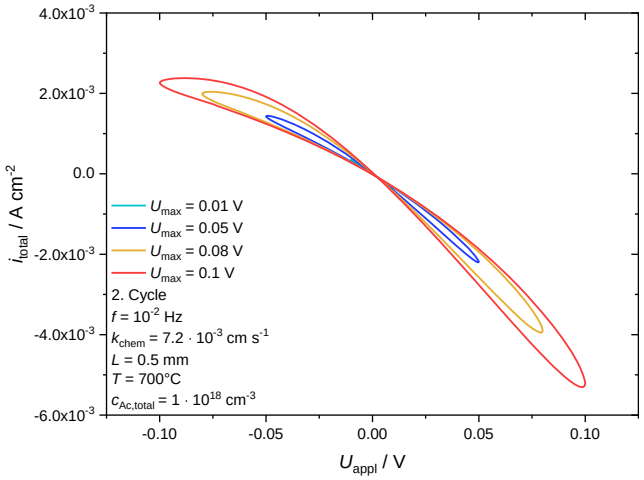


Figure 15. Simulated total current density i_{total} of the second cycle as a function of the applied voltage U_{appl} at different maximum voltages U_{max}. The following simulation setup was used: $f = 10^{-2}$ Hz, $T = 700$ °C, $c_{Ac'} = 1 \times 10^{18}$ cm^{-3}, $k_{chem} = 7.2 \times 10^{-3}$ cm s^{-1}, and $L = 0.5$ mm.

different temperatures is shown in Figure S8 and S9, Supporting Information).

In comparison to the experiments, the reproduced simulation curves show nearly the same maximum current densities in both polarity regions. Moreover, the shape of the hysteresis is similar, but slightly more curved at negative polarity than in the experiment. This may have been caused by a wide variety of outside influences during the experiment that were not taken into account in the simulations.

In conclusion, it is not possible to model the exact shape of the experimental resistive switching curves because of the different unknown outside influences during the experiment. But we could show that there is a high accordance between the simulations and the experiment. Thus, it is feasible to use the Hebb–Wagner polarization setup to perform resistive switching at perovskite-type oxides.

6. Conclusion

The resistive switching behavior of perovskite-type oxides by using the Hebb–Wagner polarization setup was investigated under different conditions. The model system of this numerical simulation is $SrTiO_3$ and the results of the simulation were verified experimentally. We could show that it is possible to switch between a high-resistive OFF and a low-resistive ON state even for thick samples ($L = 1$ mm) and low voltages ($U_{max} = 0.1$ V) depending on the applied frequency f. Here, we found that the switching time and the relaxation time of the Hebb–Wagner polarization method must be of the same order of magnitude to generate a distinct hysteresis. To simulate a realistic experimental case, a surface exchange coefficient was considered, which affects the generation of a hysteresis by lowering the optimum frequency at constant sample thicknesses. This is caused by a limited exchange of the electronic species at the RE electrode. However, it is possible to increase the frequency up to 1 MHz by reducing the sample thickness to $L = 100$ nm. It has also been shown that the limited surface exchange leads to a surface-controlled kinetics, which changes to a diffusion-controlled kinetics at larger sample thicknesses. The maximum applied voltage U_{max} mainly affects the ratio of the OFF and ON state at negative voltage values and indicates that the extent of the switching behavior can be increased by using higher voltages. In addition, the effect of a Schottky barrier at the IBE was investigated. This barrier limits the current flow between the IBE and the sample at negative voltages and thus decreases the effective voltage within the material. Therefore, the hysteresis gets smaller in the negative polarity region depending on the saturation current. However, the Schottky barrier only affects the resistive switching behavior at high voltages, when the electrons contribute most to the total conductivity.

The experiments show a distinct resistive switching behavior of single-crystalline $SrTiO_3$, which corresponds well to the simulation results. Both the shape and the dependence on different parameters are in agreement between the experiments and the simulations. This means that the numerical simulations are suitable to qualitatively predict the experimental results. The differences regarding the absolute values of the maximum current density are among others caused by the limitation of the surface

© 2023 The Authors. Advanced Engineering Materials published by Wiley-VCH GmbH

15272648, 0, Downloaded from https://onlinelibrary.wiley.com/doi/10.1002/adem.202201741 by Rwth Aachen Hochschulbibliothe, Wiley Online Library on [06/06/2023]. See the Terms and Conditions (https://onlinelibrary.wiley.com/terms-and-conditions) on Wiley Online Library for rules of use; OA articles are governed by the applicable Creative Commons License

exchange at the RE, a higher acceptor impurity of the single crystals and a constant resistance within the measuring cell, which cannot be explained yet.

Nevertheless, we could show that it is possible to induce a distinct resistive switching behavior by using the Hebb–Wagner polarization setup. Considering low sample thicknesses and a good surface exchange at the RE, the switching can be performed with low switching times (up to 10 ns), which is a very important investigation regarding the technical application of these systems. Furthermore, we emphasize that the Hebb–Wagner setup leads to a bulk switching of $SrTiO_3$ and thus does not require an initial filament formation process as often reported in the literature.

Supporting Information

Supporting Information is available from the Wiley Online Library or from the author.

Acknowledgements

This research was funded by the Deutsche Forschungsgemeinschaft (DFG) through the priority program SPP1959 "Manipulation of Matter Controlled by Electric and Magnetic Fields: Towards Novel Synthesis and Processing Routes of Inorganic Materials."

Open Access funding enabled and organized by Projekt DEAL.

Conflict of Interest

The authors declare no conflict of interest.

Data Availability Statement

The data that support the findings of this study are available from the corresponding author upon reasonable request.

Keywords

Hebb–Wagner polarization method, resistive switching, $SrTiO_3$

Received: November 30, 2022
Published online:

[1] R. Waser, M. Aono, in *Nanoscience and Technology: A Collection of Reviews from Nature Journals* (Ed: P. Rodgers), Macmillan Publishers Ltd., London, Singapore **2010**, pp. 158–165.
[2] R. Waser, R. Dittmann, G. Staikov, K. Szot, *Adv. Mater.* **2009**, *21*, 2632.
[3] I. Valov, *ChemElectroChem* **2014**, *1*, 26.
[4] A. Sawa, *Materials Today* **2008**, *11*, 28.
[5] Y. Chen, *IEEE Trans. Electron Devices* **2020**, *67*, 1420.
[6] A. Al-Haddad, C. Wang, H. Qi, F. Grote, L. Wen, J. Bernhard, R. Vellacheri, S. Tarish, G. Nabi, U. Kaiser, Y. Lei, *ACS Appl. Mater. Interfaces* **2016**, *8*, 23348.
[7] C. Yoshida, K. Tsunoda, H. Noshiro, Y. Sugiyama, *Appl. Phys. Lett.* **2007**, *91*, 223510.
[8] T. W. Hickmott, *J. Appl. Phys.* **1962**, *33*, 2669.
[9] T. W. Hickmott, *J. Appl. Phys.* **1965**, *36*, 1885.
[10] W. R. Hiatt, T. W. Hickmott, *Appl. Phys. Lett.* **1965**, *6*, 106.
[11] K. L. Chopra, *J. Appl. Phys.* **1965**, *36*, 184.
[12] A. Beck, J. G. Bednorz, C. Gerber, C. Rossel, D. Widmer, *Appl. Phys. Lett.* **2000**, *77*, 139.
[13] S. Q. Liu, N. J. Wu, A. Ignatiev, *Appl. Phys. Lett.* **2000**, *76*, 2749.
[14] K. H. Lee, Y. Mune, H. Ohta, K. Koumoto, *Appl. Phys. Express* **2008**, *1*, 15007.
[15] X. Li, H. Zhao, X. Zhou, N. Xu, Z. Xie, N. Chen, *Int. J. Hydrogen Energy* **2010**, *35*, 7913.
[16] C. Funck, A. Marchewka, C. Bäumer, P. C. Schmidt, P. Müller, R. Dittmann, M. Martin, R. Waser, S. Menzel, *Adv. Electron. Mater.* **2018**, *4*, 1800062.
[17] A. Koehl, H. Wasmund, A. Herpers, P. Guttmann, S. Werner, K. Henzler, H. Du, J. Mayer, R. Waser, R. Dittmann, *APL Mater.* **2013**, *1*, 42102.
[18] D. H. Kwon, S. Lee, C. S. Kang, Y. S. Choi, S. J. Kang, H. L. Cho, W. Sohn, J. Jo, S. Y. Lee, K. H. Oh, T. W., Noh, *Adv. Mater.* **2019**, *31*, 1901322.
[19] T. Menke, P. Meuffels, R. Dittmann, K. Szot, R. Waser, *J. Appl. Phys.* **2009**, *105*, 66104.
[20] S. A. Mojarad, J. P. Goss, K. S. K. Kwa, Z. Zhou, R. A. S. Al-Hamadany, D. J. R. Appleby, N. K. Ponon, A. O'Neill, *Appl. Phys. Lett.* **2012**, *101*, 173507.
[21] R. Muenstermann, T. Menke, R. Dittmann, R. Waser, *Adv. Mater.* **2010**, *22*, 4819.
[22] K. Szot, R. Dittmann, W. Speier, R. Waser, *Phys. Status Solidi RRL* **2007**, *1*, R86.
[23] R. Moos, K. H. Hardtl, *J. Am. Ceram. Soc.* **1997**, *80*, 2549.
[24] F. A. Kröger, H. J. Vink, *Solid State Phys.* **1956**, *3*, 307.
[25] M. H. Hebb, *J. Chem. Phys.* **1952**, *20*, 185.
[26] C. Wagner, *Z. Elektrochem.* **1956**, *60*, 4.
[27] N. Ahr, M. Martin, *Solid State Ionics* **2022**, 116057.
[28] COMSOL Multiphysics, v5.4, https://www.comsol.com, COMSOL AB, Stockholm, Sweden **2018**.
[29] M. Q. Guo, Y. C. Chen, C. Y. Lin, Y. F. Chang, B. Fowler, Q. Q. Li, J. Lee, Y. G. Zhao, *Appl. Phys. Lett.* **2017**, *110*, 233504.
[30] C. H. Jia, X. W. Sun, G. Q. Li, Y. H. Chen, W. F. Zhang, *Appl. Phys. Lett.* **2014**, *104*, 43501.
[31] C. Lenser, A. Koehl, I. Slipukhina, H. Du, M. Patt, V. Feyer, C. M. Schneider, M. Lezaic, R. Waser, R. Dittmann, *Adv. Funct. Mater.* **2015**, *25*, 6360.
[32] S. Menzel, B. Ulrich, M. Wimmer, M. Salinga, *Adv. Funct. Mater.* **2015**, *25*, 6306.
[33] J. Sun, C. H. Jia, G. Q. Li, W. F. Zhang, *Appl. Phys. Lett.* **2012**, *101*, 133506.
[34] X. Sun, G. Li, X.'a. Zhang, L. Ding, W. Zhang, *J. Phys. D: Appl. Phys.* **2011**, *44*, 125404.
[35] K. Shibuya, R. Dittmann, S. Mi, R. Waser, *Adv. Mater.* **2010**, *22*, 411.
[36] R. A. D. Souza, J. Fleig, R. Merkle, J. Maier, *Zeitung für Metallkunde* **2003**, *94*, 218.
[37] W. Weppner, *J. Solid State Chem.* **1977**, *20*, 305.
[38] R. Waser, M. Aono, *Nat. Mater.* **2007**, *6*, 833.
[39] H. B. Michaelson, *Surf. Sci.* **1977**, *48*, 4729.
[40] D. Gu, S. K. Dey, P. Majhi, *Appl. Phys. Lett.* **2006**, *89*, 82907.
[41] D. E. Eastman, *Phys. Rev. B* **1970**, *2*, 1.
[42] Y.-W. Chung, W. B. Weissbard, *Phys. Rev. B* **1979**, *20*, 3456.
[43] T. Ma, R. Jacobs, J. Booske, D. Morgan, *APL Mater.* **2020**, *8*, 71110.
[44] W. Maus-Friedrichs, M. Frerichs, A. Gunhold, S. Krischok, V. Kempter, G. Bihlmayer, *Surf. Sci.* **2002**, *515*, 499.
[45] S.O. Kasap, *Principles of Electronic Materials and Devices*, 4th ed., McGraw-Hill Education, New York **2018**.
[46] W. Schottky, *Z. Phys.* **1939**, *113*, 367.

© 2023 The Authors. Advanced Engineering Materials published by Wiley-VCH GmbH

15272648, 0, Downloaded from https://onlinelibrary.wiley.com/doi/10.1002/adem.202201741 by Rwth Aachen Hochschulbibliothe, Wiley Online Library on [06/06/2023]. See the Terms and Conditions (https://onlinelibrary.wiley.com/terms-and-conditions) on Wiley Online Library for rules of use; OA articles are governed by the applicable Creative Commons License